

# Static and dynamic properties of large polymer melts in equilibrium

Hsiao-Ping Hsu\* and Kurt Kremer†

Max-Planck-Institut für Polymerforschung, Ackermannweg 10, 55128, Mainz

We present a detailed study of the static and dynamic behavior of long semiflexible polymer chains in a melt. Starting from previously obtained fully equilibrated high molecular weight polymer melts [Zhang *et al.* ACS Macro Lett. 3, 198 (2014)] we investigate their static and dynamic scaling behavior as predicted by theory. We find that for semiflexible chains in a melt, results of the mean square internal distance, the probability distributions of the end-to-end distance, and the chain structure factor are well described by theoretical predictions for ideal chains. We examine the motion of monomers and chains by molecular dynamics simulations using the ESPResSo++ package. The scaling predictions of the mean squared displacement of inner monomers, center of mass, and relations between them based on the Rouse and the reptation theory are verified, and related characteristic relaxation times are determined. Finally we give evidence that the entanglement length  $N_{e,PPA}$  as determined by a primitive path analysis (PPA) predicts a plateau modulus,  $G_N^0 = \frac{4}{5}(\rho k_B T / N_e)$ , consistent with stresses obtained from the Green-Kubo relation. These comprehensively characterized equilibrium structures, which offer a good compromise between flexibility, small  $N_e$ , computational efficiency, and small deviations from ideality provide ideal starting states for future non-equilibrium studies.

## I. INTRODUCTION

A fundamental property of polymer melts containing long linear chains is that they are entangled. As the stiffness of chains increases, the entanglement effect becomes stronger, i.e. the entanglement length is shorter. Complex topological constraints in polymer melts play an essential role for dynamic, and rheological properties. For studying such properties and phenomena in an out-of-equilibrium state it is important to begin with a well characterized equilibrium ‘sample’ of very long polymer chains in a melt. It is the purpose of this study to provide this.

According to Flory’s argument, the excluded volume interactions become screened [1, 2] when the concentration of polymer solutions exceed the chain overlap concentration. Therefore polymer chains in a melt eventually behave statistically as ideal chains, as if excluded volume effect would no longer be important. However, Wittmer and his co-workers [3, 4] have pointed out that there are noticeable deviations from an ideal chain behavior due to the incompressibility constraint of the melt. For fully flexible polymer chains in a melt based on lattice and continuum models, bond fluctuation model (BFM) and bead-spring model, respectively, such deviations are indeed seen. This finding is confirmed by a recent Monte Carlo study of polymer melts using BFM in Ref. [5] while the deviations are less visible as the chain stiffness starts to play a role for polymers. Therefore, we provide a detailed study of the conformational properties of long bead-spring polymer chains in a melt as the chain stiffness is taken into account, where we especially study to what extent polymer chains behave as ideal chains.

It is well known that for short unentangled chains in a melt, the motion of monomers can be approximately described by the Rouse model [1, 6–8]. If the polymer chains become long enough such that the effects of entanglements start to become important, movements of chains at the intermediate time and length scales are confined to a tube-like region, created by surrounding chains and depending on the corresponding entanglement length  $N_e$ . The dynamic behavior within this time frame is well described by the tube model of de Gennes, Doi and Edwards [1, 6, 9]. Each polymer chain is assumed to move back and forth (reptation) along the contour of an imaginary tube around the so called primitive path. Although ample evidence of reptation scaling predictions is given by previous Monte Carlo and molecular dynamics simulations [10–15], a complete picture still is lacking. This is mostly due to the limitations of available equilibrated systems of huge chain length and the long relaxation times covering several orders of magnitude.

Recently, the authors of Ref. [16] developed a novel and very efficient methodology for equilibrating high molecular weight polymer melts through a sequential backmapping of a soft-sphere coarse-grained model [17, 18] from low resolution to high resolution, and finally the application of molecular dynamics (MD) simulations of the underlying bead-spring model (see Appendix). Therefore, a further investigation of the static and dynamic scaling behavior predicted by theories [1, 2, 6] for huge systems in the highly entangled regime has become easily accessible. Therefore, the aim of this paper is to give a deeper understanding of static and dynamic behavior of large semiflexible polymer chains in a melt, and compare our numerical results whenever it is possible to theoretical predictions in the literature. We mainly focus on polymer melt system containing  $n_c = 1000$  semiflexible polymer chains of sizes  $N = 500, 1000, 2000$  with the Flory characteristic ratio  $C_\infty \sim 2.88$ . The chains are modelled as standard bead-spring chains with a bond bending interactions pa-

\*Electronic address: hsu@mpip-mainz.mpg.de

†Electronic address: kremer@mpip-mainz.mpg.de

parameter  $k_\theta = 1.5$ . For details of the model we refer to the appendix. All results quoted refer to chains with a bending constant of  $k_\theta = 1.5$  unless otherwise noted. Having such big polymer melt systems at hand we have the possibility to analyze the linear viscoelasticity as characterized by the stress relaxation modulus, and estimate the entanglement length  $N_e$  from the standard expression of the plateau modulus  $G_N^0 = (4/5)(\rho k_B T / N_e)$ . It is also interesting to check whether  $N_e$  is equivalent to the estimate of  $N_{e,PPA}$  through the primitive path analysis (PPA) [19].

The outline of the paper is as follows: Sec. II describes the static conformational structures of polymer chains in a melt, and compares them to those for ideal chains. Sec. III describes the motions of polymer chains in a melt at different characteristic time scales, and verifies the scaling laws predicted by the Rouse model, and the reptation theory [1, 6, 9]. The detailed structure investigation of the primitive path of chains is given in Sec. IV. Studies of linear viscoelasticity of polymer melts are given in Sec. V. Finally, our conclusions are summarized in Sec. VI.

## II. STATIC PROPERTIES OF EQUILIBRATED POLYMER MELTS

Let us first look at the estimates of the mean square end-to-end distance and the mean square radius of gyration given by

$$\langle R_e^2 \rangle = \frac{1}{n_c} \sum_{i=1}^{n_c} \langle (\vec{r}_{i,N} - \vec{r}_{i,1})^2 \rangle, \quad (1)$$

and

$$\langle R_g^2 \rangle = \frac{1}{n_c N} \sum_{i=1}^{n_c} \left\langle \sum_{j=1}^N (\vec{r}_{i,j} - \vec{r}_{i,\text{c.m.}})^2 \right\rangle, \quad (2)$$

$$\text{with } \vec{r}_{i,\text{c.m.}} = \frac{1}{N} \sum_{j=1}^N \vec{r}_{i,j}$$

where  $\vec{r}_{i,j}$  is the position of monomer  $j$  of chain number  $i$  while  $\vec{r}_{i,\text{c.m.}}$  is the center of mass (c.m.) of the  $i$ -th polymer chain in a melt, and the average  $\langle \dots \rangle$  includes an averaging over all independent equilibrated configurations. Results of  $\langle R_e^2 \rangle / (6\ell_b^2)$  and  $\langle R_g^2 \rangle / \ell_b^2$  plotted versus  $N$  are shown in Fig. 1 for polymer melts containing  $n_c = 1000$  chains of sizes  $N = 500, 1000, \text{ and } 2000$ . Here the root-mean square bond length  $\ell_b = |\vec{b}^2|^{1/2} \approx 0.964$ . We see that  $\langle R_e^2 \rangle \propto \langle R_g^2 \rangle \propto N$ , and  $\langle R_e^2 \rangle / \langle R_g^2 \rangle \approx 6$  as one would expect for ideal chains.

The conformational behavior of individual polymer chains of size  $N$  in a melt can also be described by the probability distributions of end-to-end distance  $\vec{R}_e$  and gyration radius  $R_g$ ,  $P_N(\vec{R}_e)$  and  $P_N(R_g)$ , respectively. For ideal chains where  $\langle R_e^2 \rangle \propto N\ell_b^2$ , the probability dis-

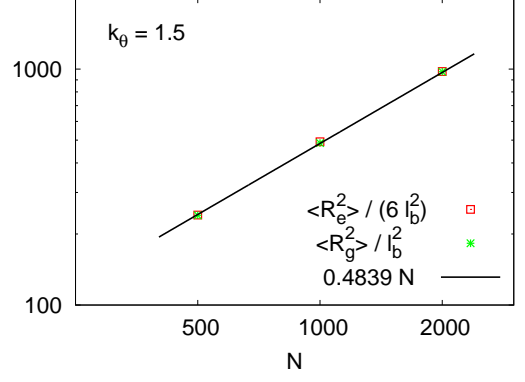


FIG. 1: Log-log plot of rescaled mean square end-to-end distance  $\langle R_e^2 \rangle / (6\ell_b^2)$  and gyration radius  $\langle R_g^2 \rangle / \ell_b^2$  versus  $N$ . The straight line indicates a fit of the power law,  $\langle R_e^2 \rangle \propto \langle R_g^2 \rangle \propto N^{2\nu}$  with  $\nu = 1/2$  for ideal chains, to the data.

tribution of  $\vec{R}_e$  is a Gaussian distribution,

$$P_N(\vec{R}_e) = \left( \frac{3}{2\pi \langle R_e^2 \rangle} \right)^{3/2} \exp \left( -\frac{3\vec{R}_e^2}{2\langle R_e^2 \rangle} \right). \quad (3)$$

Although there exists an exact theoretical prediction [2, 20, 21] for the probability distribution of  $R_g$  it is much more complicated to evaluate. However, it has been checked [5, 17, 22] that the formula suggested by Lhuillier [23] for polymer chains under good solvent conditions in  $d$ -dimensions is still a good approximation for ideal chains ( $\nu = 1/2$ ), i.e.,

$$P_N(R_g) \sim \exp \left[ -a_1 \left( \frac{\ell_b N^\nu}{R_g} \right)^{\alpha d} - a_2 \left( \frac{R_g}{\ell_b N^\nu} \right)^\delta \right] \quad (4)$$

where  $a_1$  and  $a_2$  are (non-universal) constants, and the exponents  $\alpha$  and  $\delta$  are linked to the space dimension  $d$  and the Flory exponent  $\nu$  by  $\alpha = (\nu d - 1)^{-1}$  and  $\delta = (1 - \nu)^{-1}$ . Here  $(1 + \alpha)$  is the des Cloizeaux exponent [24] for the osmotic pressure of a semidilute polymer solution, and  $\delta$  is the Fisher exponent [25] characterizing the end-to-end distance distribution.

The probability distribution of any observable  $x$  is normally obtained numerically by accumulating the histogram  $H_N(x) = \sum_{\text{config}} \delta_{x,x'}$  over all configurations and all chains of size  $N$ , and then normalizing the histogram such that

$$h_N(x) = \frac{H_N(x)}{\sum_{x'} H_N(x')} \quad \text{and} \quad \sum_x h_N(x) = 1 \quad (5)$$

In Fig. 2, we present the normalized probability distribution  $h_N(r_e)$  ( $h_N(r_g)$ ) as a function of  $r_e = (R_e^2 / \langle R_e^2 \rangle)^{1/2}$  ( $r_g = (R_g^2 / \langle R_g^2 \rangle)^{1/2}$ ) for polymer melts of three different chain sizes  $N = 500, 1000, \text{ and } 2000$ . Note that an angular average over all directions has been included in  $h_N(r_e)$ . We see the nice data collapse for both

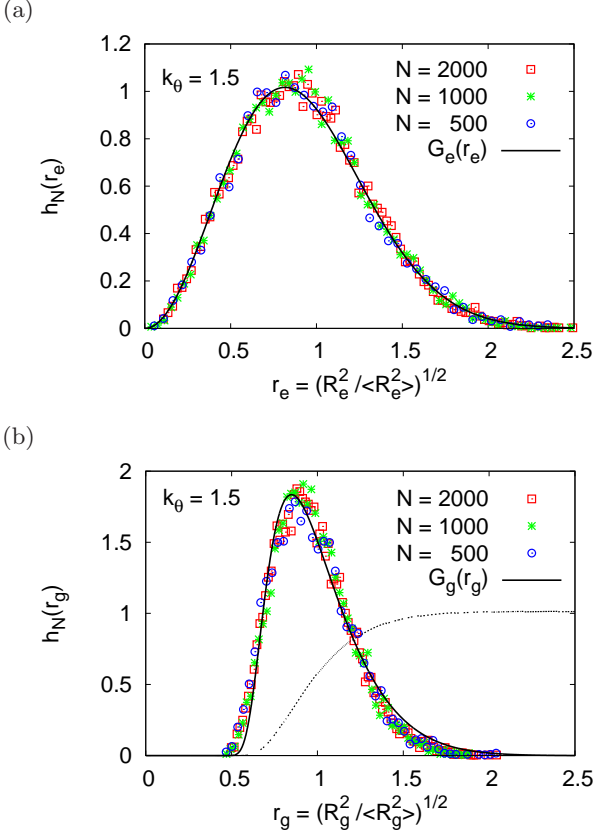


FIG. 2: Normalized probability distributions of  $r_e = (R_e^2 / \langle R_e^2 \rangle)^{1/2}$ ,  $h_N(r_e)$  (a), and  $r_g = (R_g^2 / \langle R_g^2 \rangle)^{1/2}$ ,  $h_N(r_g)$  (b), plotted versus  $r_e$ , and  $r_g$ , respectively, for polymer chains in a melt. Data are for  $N = 500, 1000$ , and  $2000$ . Theoretical predictions  $G_e(r_e)$  {Eq. (7)} and  $G_g(r_g)$  {Eq. (8)} with  $b_1 = 0.14$ ,  $b_2 = 1.52$ , and  $C_g = 7.92$  such that  $\int_0^\infty dr_g G_g(r_g) = 1$  are also shown in (a) and (b), respectively, for comparison.

$h_N(r_e)$  and  $h_N(r_g)$ , and they are described very well by the following two  $N$ -independent normalized distribution functions obtained from Eqs. (3), (4), and  $\langle R_g^2 \rangle = k\ell_b^2 N$  with  $k = 0.4839$  shown in Fig. 1,

$$G_e(r_e) = 4\pi r_e^2 \left( \frac{3}{2\pi} \right)^{3/2} \exp \left( -\frac{3r_e^2}{2} \right), \quad (6)$$

$$\int_0^\infty dr_e G_e(r_e) = 1$$

and

$$G_g(r_g) = C_g \exp(-b_1 r_g^{-\alpha d} - b_2 r_g^\delta), \quad (7)$$

$$\int_0^\infty dr_g G_g(r_g) = 1$$

where the parameters  $b_1 = a_1 k^{-\alpha d/2}$ ,  $b_2 = a_2 k^{\delta/2}$ , and the normalization factor  $C_g$  are determined numerically by a least-squares fit.

For understanding the connectivity and correlation between monomers the conformations of linear chains of

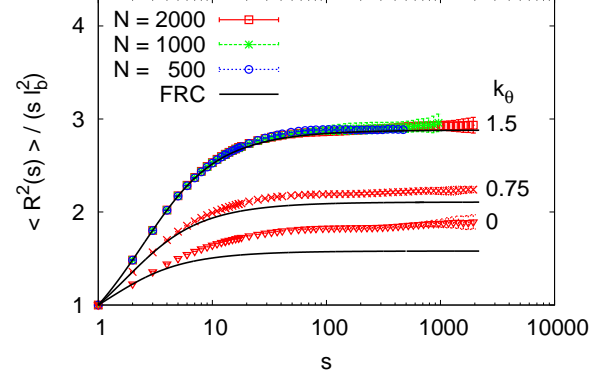


FIG. 3: Rescaled mean square internal distance,  $\langle R^2(s) \rangle / (s\ell_b^2)$ , plotted as a function of  $s$  with error bars. Three different chain sizes  $N = 500, 1000$ , and  $2000$  are chosen for  $k_\theta = 1.5$ , as indicated. For  $k_\theta = 0.75$  and  $k_\theta = 0$ , only data for  $N = 2000$  are included. The theoretical prediction for freely rotating chains (FRC) is also shown by solid curves for comparison.

contour length  $L = (N - 1)\ell_b$  in a melt are usually described by the average mean square internal distance,  $\langle R^2(s) \rangle$ ,

$$\langle R^2(s) \rangle = \left\langle \frac{1}{n_c} \sum_{i=1}^{n_c} \left[ \frac{1}{N-s} \sum_{j=1}^{N-s} (\vec{r}_{i,j} - \vec{r}_{i,j+s})^2 \right] \right\rangle, \quad (8)$$

where  $s$  is the chemical distance between the  $j^{\text{th}}$  monomer and the  $(j+s)^{\text{th}}$  monomer along the identical chain. It is generally believed that the theoretical prediction of mean square internal distance for polymer melts consisting of semiflexible chains in the absence of excluded volume effect described by a freely rotating chain model is [26]

$$\langle R^2(s) \rangle = s\ell_b^2 \left[ \frac{1 + \langle \cos \theta \rangle}{1 - \langle \cos \theta \rangle} - \frac{2\langle \cos \theta \rangle(1 - \langle \cos \theta \rangle^s)}{s(1 - \langle \cos \theta \rangle)^2} \right], \quad (9)$$

with

$$\langle \cos \theta \rangle = \langle \vec{b}_j \cdot \vec{b}_{j+1} \rangle / \ell_b^2, \quad j = 1, 2, \dots, N-1. \quad (10)$$

In the limit  $N \rightarrow \infty$ , the bond-bond orientational correlation function therefore decays exponentially as a function of chemical distance  $s$  between any two bonds along a linear chain [9, 27],

$$\langle \vec{b}_j \cdot \vec{b}_{j+s} \rangle = \ell_b^2 \langle \cos \theta(s) \rangle = \ell_b^2 \langle \cos \theta \rangle^s = \ell_b^2 \exp(-s\ell_b/\ell_p), \quad (11)$$

where  $\ell_p$  is the so-called persistence length which can be extracted from the initial decay of  $\langle \cos \theta(s) \rangle$ .

As  $s = N - 1$ , Eq. (9) gives the asymptotic behavior of the mean square end-to-end distance of a FRC equivalent

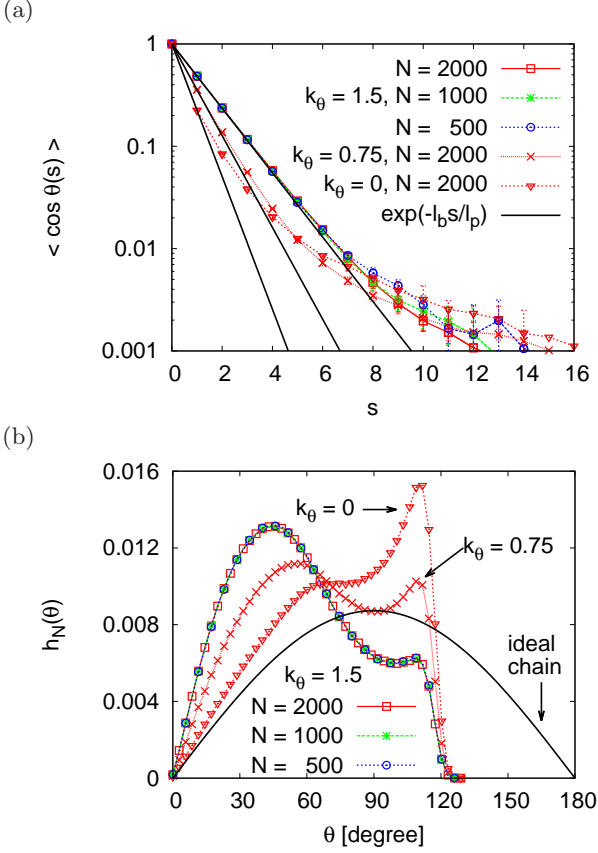


FIG. 4: (a) Semi-log plot of the bond-bond orientational correlation function  $\langle \cos \theta(s) \rangle$  vs.  $s$  with error bars. (b) Normalized probability distribution of bond angles  $\theta$ ,  $h_N(\theta)$ , plotted versus  $\theta$ . In (a), the straight lines indicate the initial exponential decay  $\exp(-\ell_b s / \ell_p)$  with  $\ell_p / \ell_b = 0.67, 0.97$ , and  $1.38$  for  $k_\theta = 0, 0.75$ , and  $1.5$ , respectively. In (b), the theoretical prediction (solid curve) for an ideal chain in a dilute solution is also shown for comparison. Data are for polymer melts containing  $n_c = 1000$  chains of  $N$  monomers.  $N = 500, 1000, 2000$  for  $k_\theta = 1.5$ , and  $N = 2000$  for  $k_\theta = 0.75, 0$ , as indicated.

to the behavior of a freely jointed chain

$$\langle R_e^2(N) \rangle = C_\infty(N-1)\ell_b^2 \text{ with } C_\infty = \frac{1 + \langle \cos \theta \rangle}{1 - \langle \cos \theta \rangle} \quad (12)$$

$$= \ell_K L = 2\ell_p L \quad (13)$$

where  $C_\infty$  is so-called Flory's characteristic ratio [26], and  $\ell_K = 2\ell_p$  is the Kuhn length.

Results of  $\langle R^2(s) \rangle$  scaled by  $(s\ell_b^2)$ , obtained by taking the average over  $\mathcal{O}(10)$  independent polymer melts containing 1000 chains to reduce fluctuations at large  $s$ , are shown in Fig. 3. For  $k_\theta = 1.5$ , we see the nice data collapse for chains of different sizes  $N$ . The universal scaling behavior for  $k_\theta = 1.5$  is nearly in perfect agreement with the theoretical prediction of  $\langle R^2(s) \rangle$  for semiflexible chains in the absence of excluded volume effect described by a freely rotating chain (FRC) model. However, a slight deviation from the predicted curve for

FRC occurs for  $N > 800$ . This deviation becomes more prominent as the flexibility of polymer chains increases due to the correlation hole effects that the correlation hole is deeper for more flexible chains. Note that here we do not take the bond-bond orientational correlation between two successive bond vectors,  $\langle \cos \theta \rangle$  in Eq. (9), as a fitting parameter [28], but rather we estimate  $\langle \cos \theta \rangle$  directly from the equilibrated configurations of polymer melts.

The correlations  $\langle \cos \theta(s) \rangle$  between two bonds along an identical chain at a chemical distance  $s$  for  $k_\theta = 1.5, 0.75, 0$  are shown in Fig. 4a. As it was clarified in Refs. [3, 22, 29], the asymptotic decay of  $\langle \cos \theta(s) \rangle$  as a function of  $s$  for dense melts and at the  $\Theta$  point is not a single exponential as predicted by Eq. (11), but rather a power law decay,  $\langle \cos \theta(s) \rangle \propto s^{-3/2}$  for  $s^* \ll s \ll N$ , due to excluded volume effects. Therefore only the initial decay of  $\langle \cos \theta(s) \rangle$  is meaningful for the estimation of the persistence length  $\ell_p$ . However, the crossover point  $s^*$  shifts to larger value of  $s$  as the chain stiffness increases, i.e. the range over which the exponential decay holds extends. We also check how the profiles of probability distribution  $P(\theta)$  of bond angles  $\theta$  vary with increasing chain stiffness. Using Eq. (5),  $P(\theta)$  is estimated by accumulating normalized histograms  $h_N(\theta)$  of  $\theta$  between two successive bonds along a chain. We see that in Fig. 4b, the distributions have a bimodal form. For fully flexible chains ( $k_\theta = 0$ ) in a melt, there exists one peak occurring at  $\theta \approx 110^\circ$  due to the competition between the excluded volume effect and the flexibility. As the chain stiffness increases ( $k_\theta$  increases), a second peak starts to develop at  $\theta < 90^\circ$ , and the position where the peak is located shifts to a smaller value of  $\theta$ . For an ideal chain in a dilute solution, one should expect that

$$P(\theta) = \frac{1}{2} \sin \theta, \quad \int_0^\pi d\theta P(\theta) = 1. \quad (14)$$

This is also shown in Fig. 4b for comparison.

The scattering from single chains in a melt in equilibrium is shown in Fig. 5. In Fig. 5a we see that  $S_c(q) \approx N \exp(-q^2 \langle R_g^2 \rangle / 3) \approx N(1 - q^2 \langle R_g^2 \rangle / 3)$  for small  $q$  ( $q \ll \frac{2\pi}{R_g}$ ,  $R_g = \sqrt{\langle R_g^2 \rangle}$ ) in the Guinier regime, then a crossover occurs to the power law of Gaussian coils (ideal chains),  $S(q) \sim q^{-1/\nu}$  with  $\nu = 1/2$  for  $\frac{2\pi}{R_g} < q < \frac{2\pi}{\ell_k}$ . Here  $\ell_k = 2\ell_p \approx 2.66$  for  $k_\theta = 1.5$  using Eq. (11). Though our chains are moderately stiff ( $k_\theta = 1.5$ ) the short range initial rigid-rod regime  $S(q) \sim q^{-1}$  for  $2\pi/\ell_k < q \ll 2\pi/\ell_b$  is hardly visible, thus allowing them still to be taken as a model for flexible polymers. In order to clarify whether single chains in a melt behave as ideal chains we show the structure factors  $S_c(q)$  in a Kratky-plot in Fig. 5b. The Debye function [1, 30–32] describing the scattering from Gaussian chains,

$$S_{\text{Debye}}(q) = 2 \frac{\eta - 1 + \exp(-\eta)}{\eta^2} \quad \text{with} \quad \eta = q^2 \langle R_g^2 \rangle, \quad (15)$$

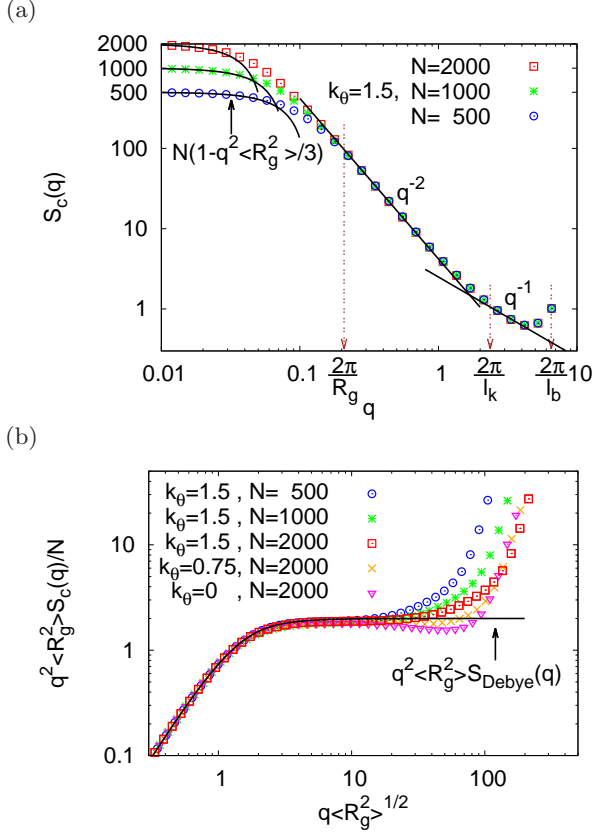


FIG. 5: (a) Structure factors of single chains in a melt,  $S_c(q)$ , plotted vs.  $q$  on log-log scales for polymer melts consisting of  $n_c = 1000$  chains of  $N = 500, 1000$ , and  $2000$  monomers, and for  $k_\theta = 1.5$ , as indicated. (b) Same data as in (a) but in a Kratky-Plot. Data for  $N = 2000$ , and  $k_\theta = 0$  and  $0.75$  are also shown, as indicated. In (a) the theoretical predictions  $S_c(q) = N(1 - q^2 \langle R_g^2 \rangle / 3)$  at the Guinier regime for small  $q$ ,  $S_c(q) \sim q^{-2}$  for a Gaussian coil, and  $S_c(q) \sim q^{-1}$  for a rigid rod are shown by solid curves for comparison. The theoretically predicted cross-over points between different regimes are pointed out by arrows. Here the root-mean-square gyration radius  $R_g = \langle R_g^2(N = 2000) \rangle^{1/2} \approx 30.15$  ( $R_e \approx 73.44$ ), the Kuhn length  $\ell_k \approx 2.66$ , and the root-mean-square bond length  $\ell_b \approx 0.964$ . In (b) the Debye function, Eq. (15), are also shown by a solid curve for comparison.

is also presented in Fig. 5b for comparison. The deviations from ideality are clearly recognized near  $q \langle R_g^2 \rangle^{1/2} \approx 20$  for rather flexible chains ( $k_\theta = 0$ ,  $k_\theta = 0.75$ ) of size  $N = 2000$ , and a minimum value is reached in the Kratky-plot as  $q$  increases, in agreement with the previous work [3, 22]. As a first conclusion one can state that polymer melts of chains with a stiffness parameter  $k_\theta = 1.5$  offer a good compromise for modeling highly

flexible polymers while at the same time minimizing deviations from ideality, which significantly impair the use of simple models for fully flexible chains.

### III. DYNAMIC PROPERTIES OF EQUILIBRATED POLYMER MELTS

The dynamic behavior of polymer chains in a melt or solution is usually characterized by the mean square displacement (MSD) of monomers. The theoretical predictions of the dynamic scaling behavior of MSD given by the reptation theory [1, 6] show that the crossover behavior occurs at different time scales, the characteristic time  $\tau_0$ , the entanglement time  $\tau_e \sim \tau_0 N_e^2$ , the Rouse time  $\tau_R \sim \tau_0 N^2$ , and the disentanglement time  $\tau_d \sim \tau_0 N^3 / N_e$  (in the ideal case where the chain length  $N$  is very large). However, all simulations and experiments support  $\tau_d \propto N^{3.4}$  due to the reason that contour length fluctuation, constrains release and correlation hole effects shift the crossover to the asymptotic behaviors to very long chains [33–36].

Three quantities describing the dynamic properties of polymer chains in a melt are listed as follows: the mean square displacement of a monomer,

$$g_1(t) \equiv \frac{1}{n_c(\frac{N}{2} + 1)} \sum_{i=1}^{n_c} \sum_{j=N/4}^{3N/4} \langle [\vec{r}_{i,j}(t) - \vec{r}_{i,j}(0)]^2 \rangle, \quad (16)$$

the mean square displacement of monomers with respect to the corresponding center of mass (c.m.),

$$g_2(t) \equiv \frac{1}{n_c N} \sum_{i=1}^{n_c} \sum_{j=1}^N \langle [(\vec{r}_{i,j}(t) - \vec{r}_{i,c.m.}(t)) - (\vec{r}_{i,j}(0) - \vec{r}_{i,c.m.}(0))]^2 \rangle, \quad (17)$$

and the mean square displacement of the center of mass

$$g_3(t) \equiv \langle [\vec{r}_{i,c.m.}(t) - \vec{r}_{i,c.m.}(0)]^2 \rangle, \quad \vec{r}_{i,c.m.}(t) = \frac{1}{N} \sum_{j=1}^N \vec{r}_{i,j}(t). \quad (18)$$

Note that in Eq. (16) only half of the monomers in the middle of each chain are considered in order to suppress the fluctuations caused by chain ends [11, 14], while all monomers in each chain  $i$  are considered in the calculation of the center of mass  $\vec{r}_{i,c.m.}(t)$  {Eq. (18)}. The corresponding scaling predictions of  $g_1(t)$ ,  $g_2(t)$ , and  $g_3(t)$  are given by [11, 37]



$$g_1(t) \sim \begin{cases} t^1, & t < \tau_0 \\ t^{1/2}, & \tau_0 < t < \tau_e \\ t^{1/4}, & \tau_e < t < \tau_R \\ t^{1/2}, & \tau_R < t < \tau_d \\ t^1, & t > \tau_d \end{cases}, \quad g_2(t) \sim \begin{cases} t^1, & t < \tau_0 \\ t^{1/2}, & \tau_0 < t < \tau_e \\ t^{1/4}, & \tau_e < t < \tau_R \\ t^{1/2}, & \tau_R < t < \tau_d \\ t^0, & t > \tau_d \end{cases}, \quad g_3(t) \sim \begin{cases} t^1, & t < \tau_e \\ t^{1/2}, & \tau_e < t < \tau_R \\ t^1, & t > \tau_R \end{cases}. \quad (19)$$

Our extensive molecular dynamics results of  $g_1(t)$ ,  $g_2(t)$ , and  $g_3(t)$  up to  $t \sim \mathcal{O}(10^7)\tau$  for polymer chains of sizes  $N = 500, 2000$  in a melt are shown in Fig. 6. The best fits of the theoretical predictions given in Eq. (19) are shown by solid lines for comparison. The characteristic time scales  $\tau_0 \approx 2.89\tau$  where  $\tau$  is the LJ time unit (see Appendix),  $\tau_e = \tau_0 N_e^2 \approx 1.98 \times 10^3 \tau$ , and  $\tau_{R,500} = \tau_0 N^2 \approx 6.44 \times 10^5 \tau$  for  $N = 500$  are determined by the intersection points of two lines from the results of  $g_1(t)$  in Fig. 6a. They correspond to the crossover points between two scaling regimes are pointed out by arrows also in Fig. 6bcd. The disentanglement time  $\tau_d \approx 2.97 \times 10^7 \tau$  is determined from the intersection between the fitting straight lines of  $g_1(t) \propto t^{1/2}$  for  $\tau_d > t > \tau_R$  and  $g_3(t) \propto t^1$  for  $t > \tau_R$ , respectively, since we should expect that  $g_1(t) = g_3(t)$  for  $t > \tau_d$ . The characteristic time  $\tau_0$  estimated from  $\tau_R = \tau_0 N^2$  for  $N = 500$  is  $2.58\tau$  which is compatible with the direct measurement. If we estimate the entanglement length  $N_e$  from characteristic time scales  $\tau_0$ ,  $\tau_e$ ,  $\tau_R$  and  $\tau_d$  determined by the scaling predictions of the mean square displacement for  $N = 500$  (Fig. 6a and 6d), we get  $N_e = (\tau_e/\tau_0)^{1/2} \approx 26(1)$  and  $N_e = N(\tau_R/\tau_d)^{1/1.4} \approx 32(2)$  if we assume that  $\tau_d = \tau_R(N/N_e)^{1.4}$ . Both estimates are consistent with results from PPA and from the relaxation plateau modulus within error bars (see Table I). The two estimates are deviating by about 10% from the expected value  $N_e = 28$ . If we fit our data with  $\tau_d = (N/N_e)\tau_R$ , we get  $N_e \sim 11$  which is underestimate. Thus our data perfectly fit experiments that  $\tau_d \propto N^{3.4}$  and show the limitations of the asymptotic theory.

According to the theoretical predictions, we see that in Fig. 6a,  $g_1(t) \approx \ell_b^2$  at  $t = \tau_0$ . At  $t = \tau_e$ ,  $g_1(t) \sim d_T^2 \approx 2\langle R_g^2(N_e) \rangle \approx (5.02\sigma)^2$  (assuming that a Rouse chain of  $N_e$  monomers is relaxed) [11, 14], where the entanglement effect starts to set in and monomers in an identical chain are restricted to move only along the contour of an imaginary tube of diameter  $d_T$  and contour length  $L_T = d_T(N/N_e)$  until reaching  $t = \tau_{R,500}$  for  $N = 500$ . Since the tube itself is a random walk with a step length  $d_T$ , the displacement of a monomer at  $t = \tau_{R,500}$  is thus  $g_1(t) \sim d_T^2(N/N_e)^{1/2} \approx 2\langle R_g^2(N_e) \rangle(N/N_e)^{1/2}$ . In the case of  $N = 2000$ , we find that our data of  $g_1(t)$  ( $g_2(t)$ ) follow the power law  $t^{1/4}$  about three decades for  $t > \tau_e$ , a much longer time window than observed so far via simulation. For  $\tau_d > t > \tau_R$ , the polymer chain slides back and forth along the tube-like regime and results in

a second  $g_1(t) \propto t^{1/2}$  regime which is predicted by the reptation theory [6]. After reaching the disentanglement time (reptation time)  $\tau_{d,500}$ , a chain has moved a distance comparable to its own size  $g_1(t) = g_3(t) \approx 3\langle R_g^2(N) \rangle$  for  $N = 500$  (see Fig. 6d). The initial tube is completely destroyed and another new tube-like regime will appear depending on the polymer chain size or polymer molecular weight. Finally monomers diffuse such that  $g_1(t) \propto t^1$  for  $t > \tau_d$ .

Results of  $g_1(t)$ ,  $g_2(t)$ , and  $Ng_3(t)$  (Fig. 6abc) show that they are all independent of  $N$  for  $t < \tau_{R,500}$ . Furthermore  $g_1(t) \cong g_2(t)$  in that regime. For  $\tau_R < t < \tau_d$ , either the size  $N = 500$  is still too short or the statistics for long relaxation time are insufficient, the expected scaling law  $g_2(t) \propto t^{1/2}$  is only seen slightly, while for  $t \approx \tau_d$ ,  $g_2(t) = \langle R_g^2(N) \rangle$  for  $N = 500$  is barely reached. However, such a proof for  $N = 2000$  or even longer chain lengths might only be possible with further improved soft and hardware [38, 39].

#### IV. COMPARISON BETWEEN THE ORIGINAL CHAIN CONFORMATIONS AND THE PRIMITIVE PATH

In order to understand the structural differences between the original path and the primitive path (pp) of polymer chains in a melt, we implement the same primitive path analysis proposed by Everaers et al. [19] based on the concept of Edwards' tube model [40] to identify the primitive path of each polymer chain in a melt [41–46]. A detailed discussion regarding to self-entanglements, local self-knot effect, and finite-size effect is given in Ref. [41, 47].

Since the motion of a chain is confined in a tube-like regime with fluctuation due to entanglements with other chains (see Sec. III), the primitive path of the chain is the contracted contour of an imaginary tube without any other chain crossing when all endpoints are fixed in space. In this analysis, topologies of chains are kept and chains are assumed to behave as random walks along their primitive paths. The mean square end-to-end distance of chains therefore remains the same as that for the

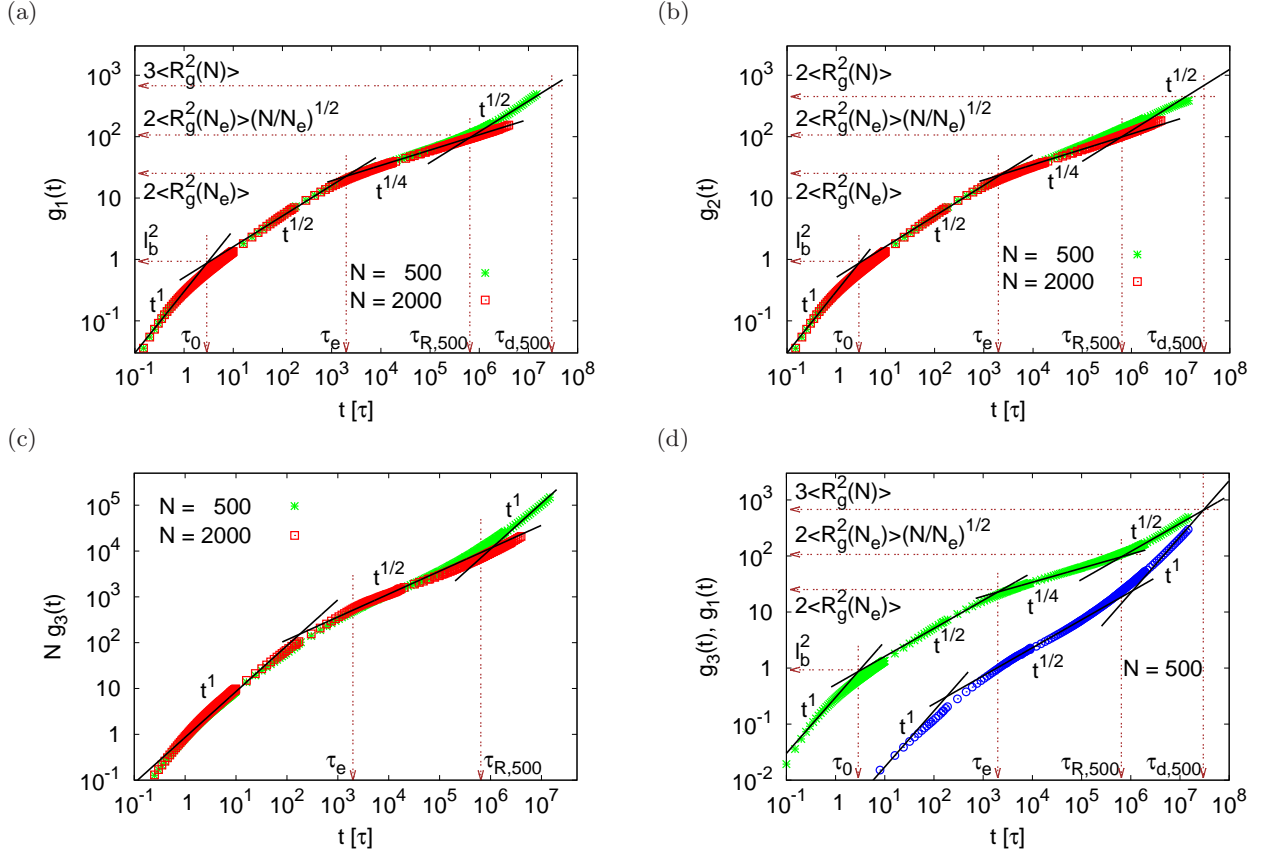


FIG. 6: Mean square displacement of inner monomers  $g_1(t)$  (a), monomers with respect to the center of mass of the corresponding chain,  $g_2(t)$  (b), and center of mass, and  $g_3(t)$  multiplied by  $N$  (c), plotted versus  $t$  for  $N = 500$  and  $N = 2000$ , as indicated. (d)  $g_1(t)$  and  $g_3(t)$  versus  $t$  for  $N = 500$ . The crossover points between two different scaling regimes are determined by the intersections of two straight lines shown in (a), and marked by arrows at  $t = \tau_0 \approx 2.89\tau$ ,  $\tau_e \approx 1.98 \times 10^3 \tau$ , and  $\tau_{R,500} \approx 6.44 \times 10^5 \tau$  while  $\tau_{d,500} \approx 2.97 \times 10^7 \tau$  is determined by the intersection of the two neighboring fitting curves for  $g_1(t)$  and  $g_3(t)$  at  $t \gg \tau_{R,500}$  in (d).

original paths of chains, i.e.,  $\langle R_{e,pp}^2 \rangle = \langle R_e^2 \rangle$ , and

$$\langle R_e^2(N) \rangle = \ell_K^{(pp)} L_{pp} = \ell_K^{(pp)} (N-1) \ell_b^{(pp)}$$

$$\text{with } \ell_b^{(pp)} = \frac{\sum_{j=1}^{N-1} |\vec{r}_{j+1} - \vec{r}_j|}{N-1}. \quad (20)$$

Here  $\ell_K^{(pp)}$  is the Kuhn length,  $L_{pp}$  is the contour length, and  $\ell_b^{(pp)}$  is the average bond length of the primitive path. The so-called entanglement length  $N_{e,PPA}$  defined by the number of monomers per Kuhn segment of the primitive path is then

$$N_{e,PPA} = \frac{\ell_K^{(pp)}}{\ell_b^{(pp)}}. \quad (21)$$

Quantitatively, the primitive paths of all polymer chains in a melt are determined by slowly cooling the system toward  $T = 0$  and minimizing the energy of the system [19, 47]. In the simulation, two ends of chains are fixed and the intrachain excluded volume interactions

as well as the bond bending interactions are switched off while the interchain interactions are kept. In the case where the intrachain excluded volume is kept, Sukumaran et. al. [41] have found that the difference of the estimate of  $N_{e,PPA}$  between these two cases is within error bars. Results of the bond-bond orientational correlation function  $\langle \cos \theta(s) \rangle$ , and the normalized histogram of bond angles  $\theta$ ,  $h_N(\theta)$  for the primitive paths of polymer chains in a melt with  $k_\theta = 1.5$  are shown in Fig. 7. The initial decay of  $\langle \cos \theta(s) \rangle$  described by an exponential decay  $\exp(-s \ell_b^{(pp)} / \ell_p^{(pp)})$  up to  $s = 80$  is shown by a dashed line with  $\ell_p^{(pp)} = \ell_K^{(pp)} / 2$ . Since the endpoints of chains are fixed, without considering the interchain interactions and thermal fluctuations, chains are stretched out when the bond springs try to reduce the average bond length from  $\ell_b = 0.964$  to  $\ell_b^{(pp)} = 0.31$ . This effect is stronger at the short length scale ( $s < 10$ ) where the result of  $\langle \cos \theta \rangle$  show some deviations from the fitting curve if we take a closer look. The stretching conformations of chains are also observed from the normalized histogram  $h_N(\theta)$  of

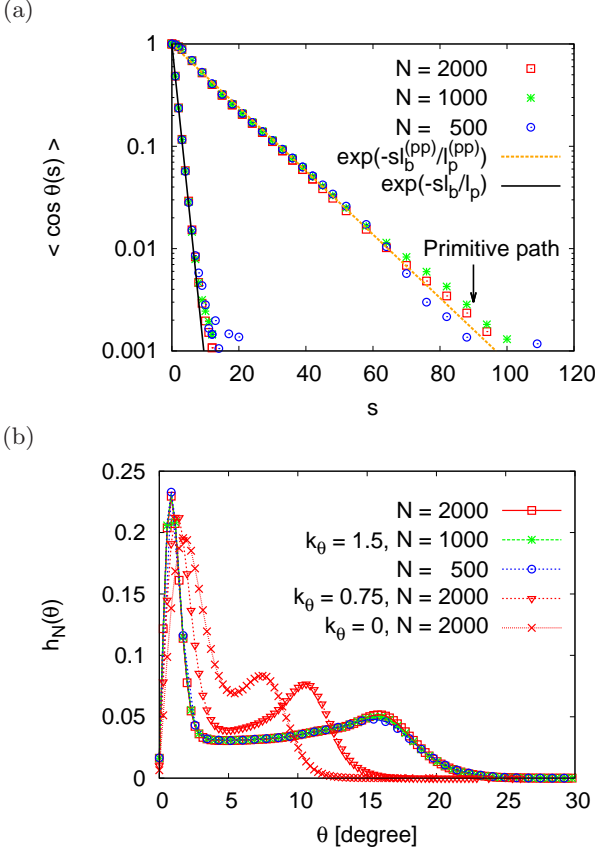


FIG. 7: (a) Semi-log plot of the bond-bond orientational correlation function  $\langle \cos \theta(s) \rangle$  vs.  $s$ . (b) Normalized probability distribution of bond angles  $\theta$ ,  $h_N(\theta)$ , plotted versus  $\theta$ . Data are for the primitive paths of polymer melts containing  $n_c = 1000$  chains of  $N$  monomers.  $N = 500, 1000, 2000$  for  $k_\theta = 1.5$ , as indicated. In (a), data for the original paths are also shown for comparison. The straight lines indicate the initial exponential decay. In (b), data for the primitive paths for  $N = 2000$ , and for  $K_\theta = 0.75, 0$  are also shown for checking the effect of chain stiffness.

bond angles  $\theta$  shown in Fig. 7. The distribution of  $\theta$  still has a bimodal form, but the range of  $\theta$  shrinks from  $[0^\circ, 130^\circ]$  (Fig. 4b) for the original paths to  $[0^\circ, 30^\circ]$  for the primitive paths in the case of  $k_\theta = 1.5$ . The distance between two peaks decreases as  $k_\theta$  decreases.

Results of the mean square internal distance  $\langle R^2(s) \rangle$  for the original and the primitive paths of polymer chains in a melt with  $k_\theta = 1.5$  are shown in Fig. 8. Since the endpoints of chains are fixed, one should expect that results of  $\langle R^2(s) \rangle$  for both paths approach to the same value with increasing  $s$ . It is indeed seen in Fig. 8. If we use  $\langle \cos \theta \rangle = \exp(-s\ell_b^{(pp)}/\ell_p^{(pp)})$  where  $\ell_p^{(pp)}/\ell_b = N_{e,PPA}/2$  with  $N_{e,PPA} \approx 28$  in Eq. (9), we see that results of  $\langle R^2(s) \rangle$  for the primitive path can still be well described by the FRC. We also check the distributions of bond length  $\ell_b^{(pp)}$  {Eq. (20)} for the primitive paths and show that the distribution is simply a normal (Gaussian) dis-

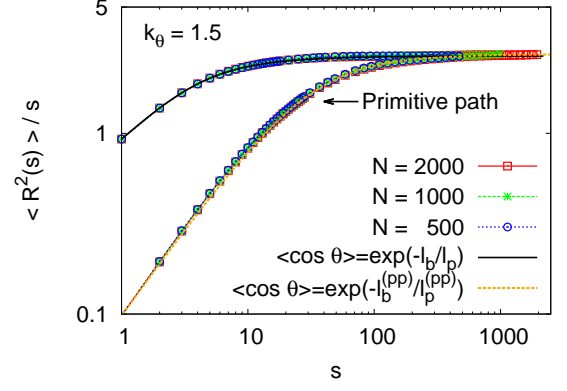


FIG. 8: Rescaled mean square internal distance,  $\langle R^2(s) \rangle/s$ , plotted as a function of  $s$ . Data are for the original paths and the primitive paths of polymer melts containing  $n_c = 1000$  chains of  $N = 500, 1000, 2000$  monomers, as indicated, and for  $k_\theta = 1.5$ . The theoretical predictions for freely rotating chains (FRC) with  $\langle \cos \theta \rangle = \exp(-\ell_b/\ell_p)$  for the original and the primitive paths, and  $\langle \cos \theta \rangle = \exp(-\ell_b^{(pp)}/\ell_p^{(pp)})$  with  $\ell_p^{(pp)} = N_{e,PPA}\ell_b^{(pp)}/2$  for the primitive path are also shown for comparison.

tribution of  $x$  ( $x = \ell_b^{(pp)}$ ) given by

$$P_N(x) = \frac{1}{\sqrt{2\pi\sigma^2(x)}} \exp\left(-\frac{(x - \langle x \rangle)^2}{2\sigma^2(x)}\right) \quad \text{and} \quad \int_0^\infty dx P_N(x) = 1, \quad (22)$$

where  $\sigma^2(x) = \langle x^2 \rangle - \langle x \rangle^2$  is the standard deviation of  $x$ , and  $\langle x \rangle$  is the mean value of  $x$  (Fig. 9). The distributions of the entanglement length  $N_{e,PPA}$ ,  $P_N(N_{e,PPA})$ , for  $N = 2000, 1000$ , and  $500$ , and for  $k_\theta = 1.5$  are shown in Fig. 9b. We see that  $P_N(N_{e,PPA} = \ell_K^{(pp)}/\ell_b^{(pp)})$  does not depend on  $N$ . The position of the peak of  $N_{e,PPA}P(N_{e,PPA})$  (fig. 9c) corresponds to the estimate [47] of  $\langle N_{e,PPA} \rangle \approx 28$ . Results of  $N_{e,PPA}$  through the PPA are listed in Table I for three different chain sizes and for  $k_\theta = 1.5$ .

## V. VISCOELASTICITY

The viscoelasticity of polymer melts is normally characterized by the stress relaxation modulus  $G(t)$  as a function of relaxation time  $t$ . For  $t < \tau_e$ ,  $G(t) \sim t^{-1/2}$  since the dynamics of chains can be described by the Rouse model while  $G(t)$  reaches a plateau value  $G_N^0 = (4/5)(\rho k_B T/N_e)$  depending on the entanglement length, or the molecular weight between entanglements predicted by the reptation theory [6, 48] for  $\tau_e < t \ll \tau_d$  where chains are assumed to move in a tube-like regime due to entanglements. Finally, entangled chains are relaxed for  $t > \tau_d$  and  $G(t)$  starts to deviate from the plateau.



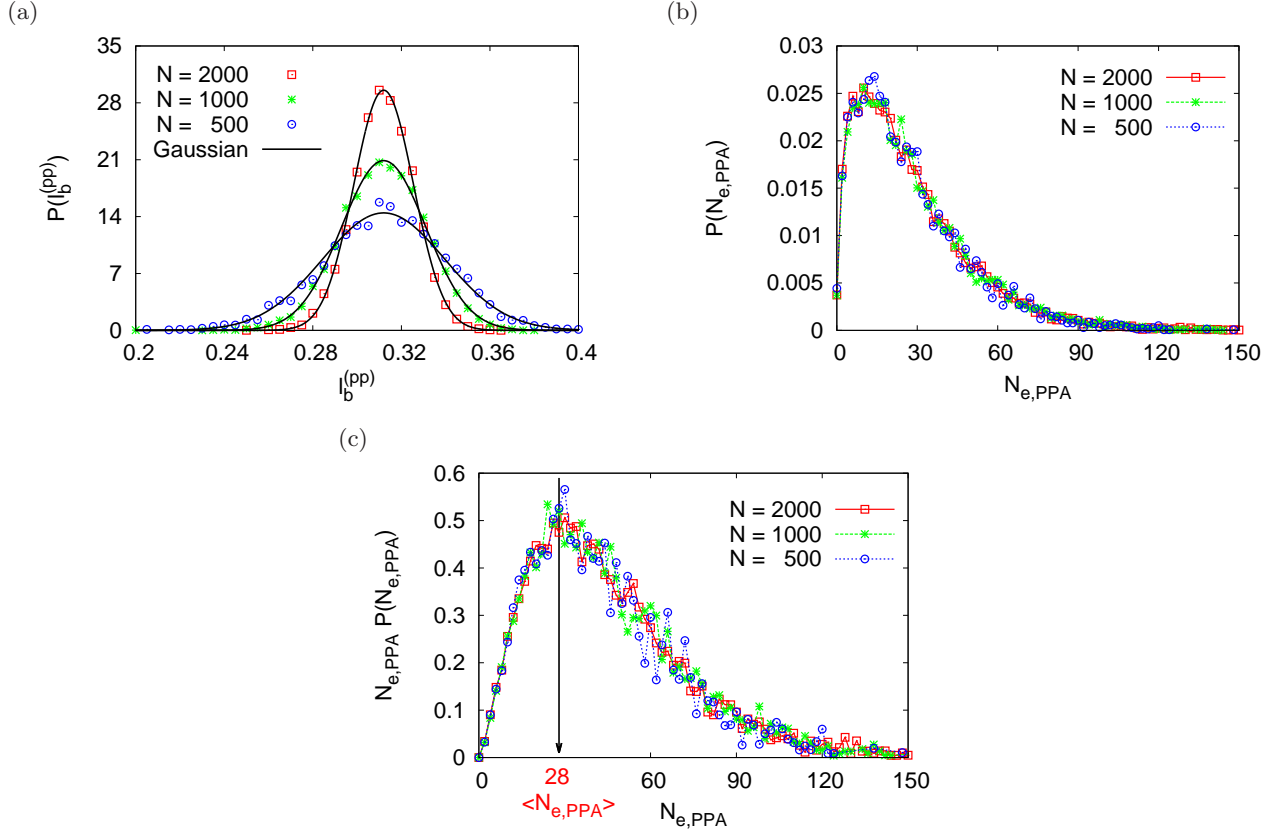


FIG. 9: (a) Normalized probability distributions of bond length  $\ell_b^{(pp)}$  of the primitive paths,  $P(\ell_b^{(pp)})$ . (b) Normalized probability distributions of the entanglement lengths  $N_{e,PPA}$ ,  $P(N_{e,PPA})$ . (c) Same data as in (b) but multiplied by  $N_{e,PPA}$ . The peak of  $N_{e,PPA}P(N_{e,PPA})$  indicates the estimate of entanglement length  $\langle N_{e,PPA} \rangle \approx 28$ . Data are for  $N = 500, 1000$ , and  $2000$ , as indicated, and for  $k_\theta = 1.5$ .

In order to clarify whether the entanglement length  $N_e$  estimated from stresses  $\sigma(t)$  using the standard expression of the plateau modulus  $G_N^0 = (4/5)(\rho k_B T / N_e)$  is equivalent to  $N_{e,PPA}$  determined through PPA mentioned in Sec. IV, we perform MD simulations to estimate the stress relaxation modulus  $G(t)$ . Two meth-

ods are considered here. One is from the stress autocorrelation function (SAF) of off-diagonal elements of the preaveraged stress tensor for fully equilibrated polymer melts [49, 50]. The components of stress tensor taking the pairwise potential  $U_{ij}$  and the three-body potential  $U_{ijk}$  into account are defined via the virial theorem:

$$\begin{aligned} \sigma_{\alpha\beta}(t) = & -\frac{1}{V} \left( \sum_{i=1}^{n_c N} m_i v_i^{(\alpha)} v_i^{(\beta)} + \frac{1}{2} \sum_{i,j=1}^{n_c N} f_{ij}^{(\alpha)} r_{ij}^{(\beta)} \right) \\ & + \frac{1}{6V} \sum_{i,j,k=1}^{n_c N} \left( \frac{r_{ij}^{(\alpha)} r_{ij}^{(\beta)}}{r_{ij}} \frac{\partial U_{ijk}}{\partial r_{ij}} + \frac{r_{jk}^{(\alpha)} r_{jk}^{(\beta)}}{r_{jk}} \frac{\partial U_{ijk}}{\partial r_{jk}} + \frac{r_{ki}^{(\alpha)} r_{ki}^{(\beta)}}{r_{ki}} \frac{\partial U_{ijk}}{\partial r_{ki}} \right) \end{aligned} \quad (23)$$

where  $m_i$  and  $v_i^\alpha$  are the mass and the  $\alpha$ th component of the velocity vector of the  $i$ th bead, respectively, and  $f_{ij}^{(\alpha)} \equiv -r_{ij}^{(\alpha)} \frac{\partial U_{ij}}{\partial r_{ij}}$  is the  $\alpha$ th component of the force vector acting on the  $i$ th bead by the  $j$ th bead. Using the

Green-Kubo relationship [51], the stress relaxation modulus

$$G(t) = (G_{xy}(t) + G_{xz}(t) + G_{yz}(t))/3 \quad (24)$$

TABLE I: Estimates of the entanglement lengths  $N_e$  from relaxation plateau modulus  $G_N^0$  and  $N_{e,PPA}$  from the primitive path analysis for polymer chains of sizes  $N = 2000, 1000$ , and  $500$  in a melt and for  $k_\theta = 1.5$ .

$N$	$N_e(\text{plateau})$	$N_{e,PPA}$
2000	$28 \pm 2$	$28.01 \pm 1.06$
1000	$26 \pm 3$	$28.30 \pm 1.38$
500	$28 \pm 3$	$27.60 \pm 1.45$

where the off-diagonal element  $G_{\alpha\beta}(t) = (V/k_B T) \text{SAF}_{\alpha\beta}(t)$ . In order to reduce the strong noise in SAF [49, 50],  $\text{SAF}_{\alpha\beta}(t)$  is defined by

$$\text{SAF}_{\alpha\beta}(t) = \langle \bar{\sigma}_{\alpha\beta}(t) \bar{\sigma}_{\alpha\beta}(0) \rangle \quad (25)$$

where the preaveraged stress tensor

$$\bar{\sigma}_{\alpha\beta}(t) = \frac{1}{N_t} \sum_{k=1}^{N_t} \sigma_{\alpha\beta}(t + k\delta t). \quad (26)$$

In our simulations, we choose  $N_t = 100$  MD steps with the time step  $\delta t = 0.01[\tau]$ .

The other method is to measure the normal stress decay  $\sigma_{norm}(t)$  after deforming polymer chains in a melt by a small step strain elongation, since linear viscoelastic properties are associated with near equilibrium measurements of the system where the configurations of polymer chains are not moved far away from their equilibrium states. In our simulations, this is done by applying  $N_{cycles}$  cycles of uniaxial elongation to deform the simulation box with a strain rate  $\tau_R^{-1} < \dot{\epsilon} < \tau_e^{-1}$  (holding each chain in a tube-like regime) at each cycle such that at the end the simulation box is elongated in the  $x$ -direction ( $L_x = \lambda L$ ), but shrunk in the  $y$ -,  $z$ -directions ( $L_y = L_z = L/\sqrt{\lambda}$ ). Here the volume of the simulation box is kept fixed,  $V = L^3$ , and the stretch ratio  $\lambda = (1.02)^{N_{cycles}} \approx 1.2$  with  $N_{cycles} = 9$  such that the system is in the linear viscoelastic regime. Using the stress-strain formulas for classical rubber elasticity [52], the stress relaxation modulus

$$G(t) = \frac{\sigma_{norm}(t)}{\lambda^2 - 1/\lambda} = \frac{(\sigma_{xx} - \frac{1}{2}(\sigma_{yy} + \sigma_{zz}))}{\lambda^2 - 1/\lambda}. \quad (27)$$

Results of  $G(t)$  scaled by  $G_N^0$  with  $N_e$  estimated by the plateau value of  $G(t)$  are shown in Fig. 10. The estimates of  $N_e$  are also listed in Table I. They are in perfect agreement with the estimates through PPA within error bars. In Fig. 10a,  $G(t)$  is estimated from Eqs. (24)-(26) for polymer melts consisting of  $n_c = 1000$  chains of sizes  $N = 500, 1000$ , and  $2000$ , and for  $k_\theta = 1.5$ . Due to the difference between microscopic structures of independent equilibrated polymer melts, we observe that the plots of  $G(t)$  as a function of  $t$  show slightly different scenarios for different sets of data (not shown). Therefore, besides taking the preaverage of  $\sigma_{\alpha\beta}$  for the estimate of  $G(t)$ , we

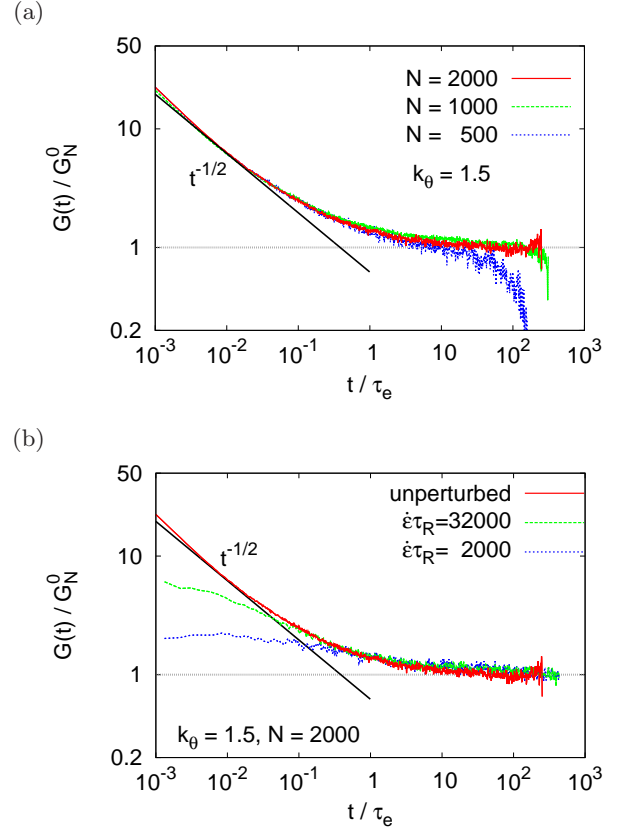


FIG. 10: (a) Stress relaxation modulus  $G(t)$  scaled by  $G_N^0 = (4/5)\rho k_B T/N_e$  plotted as a function of  $t$  from SAF {Eq. (25)} using the Green-Kubo relation. (b) Same data for  $N = 2000$  as shown in (a), and  $G(t)$  obtained from stress response to strain {Eq. (27)} after an uniaxial elongation with two different strain rates  $\dot{\epsilon}$ , as indicated. Values of  $N_e$  extracted from  $G_N^0$  in (a) for three choices of  $N$  are listed in Table I.

shall also take the average of  $G(t)$  over  $\mathcal{O}(10)$  independent sets of data although our systems are quite large. For  $t < \tau_e$ , the scaling law  $G(t) \sim t^{-1/2}$  predicted by the Rouse model is verified. As  $t$  increases, the curves of  $G(t)$  for three different sizes  $N$  first reach a plateau for  $\tau_e < t \ll \tau_d$ , then start to deviate from it depending on the chain size  $N$ . Since  $\tau_d \sim N^{3.4}$ , the range over which  $G(t) \approx \text{constant}$  extends with increasing  $N$ . However, in Fig. 10b, we only focus on the case of  $N = 2000$  and compare the results of  $G(t)$  obtained from two different measurements, Eqs (24) and (27). For the second measurement, two values of the strain rate  $\dot{\epsilon}$  are chosen,  $\dot{\epsilon}\tau_R = 2000$  and  $\dot{\epsilon}\tau_R = 32000$ . We see that  $G(t)$  only depends on  $\dot{\epsilon}$  for  $t < t_e$ . For  $t > t_e$ , results of  $G(t)$  estimated from the normal stress tensor  $\sigma_{norm}(t)$  are consistent with the estimates from SAF( $t$ ).

## VI. CONCLUSION

In this paper, we have studied bead-spring chains in a melt at a monomer density  $\rho = 0.85$  by extensive molecular dynamics simulations using the ESPResSo++ package [53]. We investigate the static and dynamic properties of polymer chains in a melt. For fully equilibrated large polymer melts, we observe that for moderately stiff chains ( $k_\theta = 1.5$ ), the ratio  $\langle R_e^2 \rangle / \langle R_g^2 \rangle \approx 6$  as expected for ideal chains. For fully flexible chains ( $k_\theta = 0$ ), results of the mean square internal distance  $\langle R^2(s) \rangle$  show remarkable deviations from the freely rotating chain model describing the behavior of ideal chains, while the deviations are diminished as the stiffness of chains increases. For  $k_\theta = 1.5$ ,  $\langle R^2(s) \rangle$  is in perfect agreement with FRC up to  $N \approx 800$ , while a slight deviation occurs for  $N > 800$  due to the correlation hole effect. Results of the probability distributions of reduced end-to-end distance  $r_e = (R_e^2 / \langle R_e^2 \rangle)^{1/2}$ , and reduced gyration radius  $r_g = (R_g^2 / \langle R_g^2 \rangle)^{1/2}$  for polymer chains in a melt for various values of  $N$  and for  $k_\theta = 1.5$  show the nice data collapse, and are described by universal functions, Eqs. (7) and (8), for ideal chains. A detailed investigation of the standard structure factor  $S_c(q)$  for single chains in a melt for  $k_\theta = 0, 0.75$ , and  $1.5$  is also given. Results of  $S_c(q)$  presented in a Kratky-plot show that there exists a significant deviation from the Debye function for Gaussian chains at the intermediate values of  $q$  as observed by Wittmer et al. [3], and Hsu [22], while for  $k_\theta = 1.5$ , it is very well described by the Debye function. We have also seen that the probability distributions of bond angles for  $k_\theta > 0$  have a bimodal form which is very different from the distribution for ideal chains {Eq. (14)}, and the positions of two peaks depend on the stiffness of chains. All these findings support the idea that polymer chains in a melt are described by ideal chains to some extent. The stiffer the chains of fixed size in a melt, the more ideal the chain.

From our extensive molecular dynamics simulations, we have provided evidence for the crossover behavior of the mean square displacements  $g_1(t)$ ,  $g_2(t)$ , and  $g_3(t)$  between several characteristic time scales,  $\tau_0$ ,  $\tau_e$ ,  $\tau_R$ , and  $\tau_d$ , as predicted by the Rouse model, and the reptation theory [1, 6, 9]. Especially, our results for  $N = 2000$  strongly support the reptation theory and the scaling law  $g_1(t) = g_2(t) \propto t^{1/4}$  for  $\tau_e < t < \tau_R$ . We also see that the corresponding values of the mean square displacement of a monomer,  $g_1(t)$ , at  $\tau_0$ ,  $\tau_e$ ,  $\tau_R$ , and  $\tau_d$ , show that the theoretical predictions are not only verified qualitatively, but also quantitatively. The entanglement length  $N_e$  determined from the estimates of  $\tau_0$ ,  $\tau_e$  and  $\tau_d$  is not affected by the chain size, and the estimates of  $N_e$  are consistent with the estimates through the primitive path analysis, and the plateau modulus obtained from the stresses (Table I).

Also a direct comparison between the original paths and the primitive paths (obtained through the primitive path analysis) of polymer chains in a melt is presented in

this work. Results of the bond-bond orientational correlation function and the mean square internal distance of chains verify the assumption that chains behave as random walks along their primitive paths. The Kuhn length  $\ell_K^{(pp)}$  of the primitive path is larger than  $\ell_K$  of the original path. The probability distribution of the average bond length along the primitive paths shows a normal Gaussian distribution. The peak of the first moment of the probability distribution of the entanglement length,  $N_{e,PPA}P(N_{e,PPA})$  corresponds to the expected value of  $\langle N_{e,PPA} \rangle$ .

Finally, the stress relaxation modulus  $G(t)$  which describes viscoelasticity of polymer melts is estimated. From the stress autocorrelation function (SAF) of off-diagonal elements using the Green-Kubo relation, and the normal stress tensor after applying an uniaxial elongation but still keeping the system in a linear regime, we verify the Rouse behavior,  $G(t) \sim t^{-1/2}$  for  $t < \tau_e$ . We also see that  $G(t)$  reaches a plateau value, and the plateau stays longer as the size of chains increases as predicted by the reptation theory [1, 6, 9]. Moreover, we show that using the standard expression of plateau modulus  $G_N^0 = (4/5)(\rho k_B T / N_e)$ , the estimate of the entanglement  $N_e$  from the stresses is equivalent to  $N_{e,PPA}$  through PPA.

All our results show that the coarse-grained bead-spring model is an ideal model for understanding the properties of fully equilibrated polymer chains in a melt from various aspects. It marks a good compromise between chain flexibility, and small entanglement length. While the flexibility allows for relatively large timesteps and the application of recently developed equilibration schemes the moderate stiffness warrants small deviations from ideality and at the same time relatively small entanglement lengths, which are decisive for comparably small, though still huge, relaxation times. Therefore, we expect that this model can serve as an optimal test case, where one can gain insight into non-linear viscoelasticity regime for large polymer melts by non-equilibrium molecular dynamics simulations.

## ACKNOWLEDGMENT

This work has been supported by European Research Council under the European Union's Seventh Framework Programme (FP7/2007-2013)/ERC Grant Agreement No. 340906-MOLPROCOP. We are grateful to G. S. Grest for stimulating discussions. We also thank G. Zhang for providing the configurations of large equilibrated polymer melt in equilibrium, K. Ch. Daoulas for helpful discussion, T. Stuehn and L. A. Moreira for assistance with the ESPResSo++ package, and A. C. Fogarty for a critical reading of the manuscript. We are also grateful to the NIC Jülich for a generous grant of computing time at the Jülich Supercomputing Centre (JSC), and the Max Planck Computing and Data Facility (MPCDF).

## APPENDIX

Polymer melts consisting of  $n_c$  chains of  $N$  monomers in a melt are described by the standard bead-spring model [11] at a volume fraction  $\phi = 0.85$  for our work here. In this model, the excluded volume interactions between bonded and non-bonded monomers at a distance  $r$  are considered by the truncated and shifted Lennard-Jones (LJ) potential, i.e., Weeks-Chandler-Andersen (WCA) potential,

$$U_{\text{LJ}}(r) = \begin{cases} 4\varepsilon \left[ \left( \frac{\sigma}{r} \right)^{12} - \left( \frac{\sigma}{r} \right)^6 + \frac{1}{4} \right] & , r \leq r_{\text{cut}} \\ 0 & , r > r_{\text{cut}} \end{cases} \quad (28)$$

where  $\varepsilon$  denotes the pairwise interaction energy, and  $r_{\text{cut}} = 2^{1/6}\sigma$  is a cut-off such that  $U_{\text{LJ}}(r_{\text{cut}}) = 0 = \min.\{U_{\text{LJ}}(r)\}$ . The bond length  $|\vec{b}_j| = |\vec{r}_{j+1} - \vec{r}_j|$  between any two connected monomers  $j$  and  $j+1$  of size  $\sigma$  and mass  $m$  along a chain is controlled by the finitely extensible nonlinear elastic (FENE) potential

$$U_{\text{FENE}}(r) = \begin{cases} -\frac{k}{2}R_0^2 \ln \left[ 1 - \left( \frac{r}{R_0} \right)^2 \right] & , r \leq R_0 \\ \infty & , r > R_0 \end{cases} \quad (29)$$

where the force constant  $k = 30\varepsilon/\sigma^2$ , and the maximum

value of bond length  $R_0 = 1.5\sigma$ . The chain stiffness is dominated by the bending potential depending on the bond angle  $\theta$  between the sequential bonds along a chain itself and the strength of the bending factor  $k_\theta$ ,

$$U_{\text{bend}}(\theta) = k_\theta(1 - \cos\theta) \quad (30)$$

The ESPResSo++ package [53] is used to perform the standard MD with Langevin thermostat including a friction constant  $\Gamma = 0.5\tau^{-1}$  where  $\tau = \sigma(m/\varepsilon)^{1/2}$ , and random force  $\vec{f}_i^R$  that

$$m \frac{d^2 \vec{r}_i}{dt^2} = -\nabla(U_{\text{LJ}} + U_{\text{FENE}} + U_{\text{bend}}) - \Gamma \frac{d\vec{r}_i}{dt} + \vec{f}_i^R(t) \quad (31)$$

and

$$\langle \vec{f}_i^R(t) \cdot \vec{f}_j^R(t') \rangle = 6k_B T \Gamma \delta_{ij} \delta(t - t'). \quad (32)$$

Here the temperature  $T = 1\varepsilon/k_B$ ,  $k_B$  is the Boltzmann factor, and  $\sigma = m = 1$ , and the basic time step  $\Delta t$  for the integration is  $0.01\tau$  throughout the whole paper. In the primitive path analysis {Sec. IV}, we set the temperature  $T = 0.001\varepsilon/k_B$  (close to zero), the basic time step  $\Delta t = 0.006$ , the friction constant  $\Gamma = 20\tau^{-1}$  during the first  $10^3$  MD steps, and  $\Gamma = 0.5\tau^{-1}$  after the first  $10^3$  steps [41, 47].

- 
- [1] P. G. de Gennes, *Scaling Concepts in polymer physics* (Cornell University Press: Ithaca, New York, 1979).
  - [2] H. Yamakawa, *Modern theory of polymer solutions* (Harper and Row, New York, 1971).
  - [3] J. P. Wittmer, P. Beckrich, A. Johner, A. N. Semenov, S. P. Obukhov, H. Mayer, and J. Baschnagel, *EPL* **77**, 56003 (2007).
  - [4] J. P. Wittmer, A. Cavallo, J. E. Z. H. Xu, P. Políńska, N. Schulmann, H. Meyer, J. Farago, A. Johner, S. P. Obukhov, and J. Baschnagel, *J. Stat. Phys.* **145**, 1017 (2011).
  - [5] H.-P. Hsu, *J. Chem. Phys.* **141**, 164903 (2014).
  - [6] M. Doi and S. Edwards, *The theory of polymer dynamics* (Oxford University Press: New York, 1986).
  - [7] J. T. Kalathi, S. K. Kumar, M. Rubinstein, and G. S. Grest, *Macromolecules* **47**, 6925 (2014).
  - [8] J. T. Kalathi, S. K. Kumar, M. Rubinstein, and G. S. Grest, *Soft Matter* **11**, 4123 (2015).
  - [9] M. Rubinstein and R. H. Colby, *Polymer Physics* (Oxford University Press, Oxford, 2003).
  - [10] A. Baumgärtner and K. Binder, *J. Chem. Phys.* **75**, 2994 (1981).
  - [11] K. Kremer and G. S. Grest, *J. Chem. Phys.* **92**, 5057 (1990).
  - [12] W. Paul, K. Binder, D. W. Heermann, and K. Kremer, *J. Chem. Phys.* **95**, 7726 (1991).
  - [13] J. Wittmer, W. Paul, and K. Binder, *Macromolecules* **25**, 7211 (1992).
  - [14] K. Kremer and G. S. Grest, *J. Chem. Soc. Faraday Trans* **88**, 1707 (1992).
  - [15] A. Kopf, B. Dünweg, and W. Paul, *J. Chem. Phys.* **107**, 6945 (1997).
  - [16] G. Zhang, L. A. Moreira, T. Stuehn, K. C. Daoulas, and K. Kremer, *ACS Macro Lett.* **3**, 198 (2014).
  - [17] T. Vettorel, G. Besold, and K. Kremer, *Soft Matter* **6**, 2282 (2010).
  - [18] G. Zhang, K. C. Daoulas, and K. Kremer, *Macromol. Chem. Phys.* **214**, 214 (2013).
  - [19] R. Everaers, S. K. Sukumaran, G. S. Grest, C. Svaneborg, A. Sivasubramanian, and K. Kremer, *Science* **303**, 823 (2004).
  - [20] H. Fujita and T. Norisuye, *J. Chem. Phys.* **52**, 1115 (1970).
  - [21] A. R. Denton and M. Schmidt, *J. Phys.: Condens. Matter* **14**, 12051 (2002).
  - [22] H.-P. Hsu, *J. Chem. Phys.* **141**, 234901 (2014).
  - [23] D. Lhuillier, *J. Phys. France* **49**, 705 (1988).
  - [24] J. des Cloizeaux, *J. Phys. France* **36**, 281 (1975).
  - [25] M. E. Fisher, *J. Chem. Phys.* **44**, 616 (1966).
  - [26] P. J. Flory, *Statistical Mechanics of Chain Molecules* (Wiley, New York, 1969).
  - [27] A. Y. Grosbeg and A. R. Khokhlov, *Statistical Physics of Macromolecules* (AIP Press, NY, 1994).
  - [28] R. Auhl, R. Everaers, G. S. Grest, K. Kremer, and S. J. Plimpton, *J. Chem. Phys.* **119**, 12718 (2003).
  - [29] H.-P. Hsu, W. Paul, and K. Binder, *Macromolecules* **20**, 510 (2010).
  - [30] J. D. Cloizeaux and G. Jannink, *Polymers in Solution: Their Modeling and Structure* (Clarendon, Oxford, 1990).

- [31] L. Schäfer, *Excluded Volume Effects in Polymer Solutions as Explained by the Renormalization Group* (Springer, Berlin, 1999).
- [32] J. S. Higgins and H. C. Benoit, *Polymers and Neutron Scattering* (Clarendon, Oxford, 1994).
- [33] M. Doi, J. Polym. Sci. Polym. Phys. Ed. **21**, 667 (1983).
- [34] S. T. Milner and T. C. B. McLeish, Phys. Rev. Lett. **81**, 725 (1998).
- [35] T. C. B. McLeish, Adv. Phys. **51**, 1379 (2002).
- [36] A. E. Likhtman and T. C. B. McLeish, Macromolecules **35**, 6332 (2002).
- [37] M. Pütz, K. Kremer, and G. S. Grest, Europhys. Lett. **49**, 735 (2000).
- [38] J. A. Anderson, C. Lorenz, and A. Travesset, J. Comput. Phys. **227**, 5342 (2008).
- [39] J. Glaser, T. D. Nguyen, J. A. Anderson, P. Lui, F. Spiga, J. A. M. adn D. C. Morse, and S. C. Glotzer, Comput. Phys. Comm. **192**, 97 (2015).
- [40] S. F. Edwards, Proc. Phys. Soc. **91**, 513 (1967).
- [41] S. K. Sukumaran, G. S. Grest, K. Kremer, and R. Everaers, J. Polym. Sci. B **43**, 917 (2005).
- [42] M. Kröger, Comput. Phys. Comm. **168**, 209 (2005).
- [43] S. Shanbhag and R. G. Larson, Phys. Rev. Lett. **94**, 076001 (2005).
- [44] C. Tzoumanekas and D. N. Theodorou, Macromolecules **39**, 4592 (2006).
- [45] R. S. Hoy, K. Foteinopoulou, and M. Kröger, Phys. Rev. E **80**, 031803 (2009).
- [46] R. Everaers, Phys. Rev. E **86**, 022801 (2012).
- [47] L. A. Moreira, G. Zhang, F. Müller, T. Stuehn, and K. Kremer, Macromol. Theory Simul. **24**, 419 (2015).
- [48] M. Doi, J. Polym. Sci. Polym. Phys. Ed. **18**, 1005 (1980).
- [49] W. B. Lee and K. Kremer, Macromolecules **42**, 6270 (2009).
- [50] W. B. Lee, J. Halverson, and K. Kremer, Macromolecules **43**, 3984 (2010).
- [51] S. Sen, S. K. Kumar, and P. Keblinski, Macromolecules **38**, 650 (2005).
- [52] L. R. G. Treloar, *The physics of Rubber Elasticity* (Clarendon Press, Oxford, 1986).
- [53] J. D. Halverson, T. Brandes, O. Lenz, A. Arnold, S. Bevc, V. Starchenko, K. Kremer, T. Stuehn, and D. Reith, Comput. Phys. Comm. **184**, 1129 (2013).